Magnetic ionization-thermal instability

A. E. Dudorov[1]⋆, C. E. Stepanov[1], S. O. Fomin[1]†, and S. A. Khaibrakhmanov[1,2]‡

[1] *Theoretical Physics Department, Chelyabinsk State University, Br. Kashirinykh St., 129, Chelyabinsk, 454001, Russia*
[2] *Ural Federal University, 51 Lenin str., Ekaterinburg 620000, Russia*

ABSTRACT

Linear analysis of the stability of diffuse clouds in the cold neutral medium with uniform magnetic field is performed. We consider that gas in equilibrium state is heated by cosmic rays, X-rays and electronic photoeffect on the surface of dust grains, and it is cooled by the collisional excitation of fine levels of the C II. Ionization by cosmic rays and radiative recombinations is taken into account. A dispersion equation is solved analytically in the limiting cases of small and large wave numbers, as well as numerically in the general case. In particular cases the dispersion equation describes thermal instability of Field (1965) and ionization-coupled acoustic instability of Flannery and Press (1979). We pay our attention to magnetosonic waves arising in presence of magnetic field, in thermally stable region, $35 \leq T \leq 95$ K and density $n \lesssim 10^3 \, \mathrm{cm}^{-3}$. We have shown that these modes can be unstable in the isobarically stable medium. The instability mechanism is similar to the mechanism of ionization-coupled acoustic instability. We determine maximum growth rates and critical wavelengths of the instability of magnetosonic waves depending on gas temperature, magnetic field strength and the direction of wave vector with respect to the magnetic field lines. The minimum growth time of the unstable slow magnetosonic waves in diffuse clouds is of $4 - 60$ Myr, minimum and the most unstable wavelengths lie in ranges $0.05 - 0.5$ and $0.5 - 5$ pc, respectively. We discuss the application of considered instability to the formation of small-scale structures and the generation of MHD turbulence in the cold neutral medium.

Key words: ISM: clouds – instabilities – magnetic fields

1 INTRODUCTION

The interstellar medium (ISM) in the Galaxy consists of three phases in a state of dynamical equilibrium (McKee & Ostriker 1977): the cold neutral medium (CNM) with $T < 100$ K, the warm intercloud medium with $T \approx 8000$ K, and the hot coronal gas with $T \approx 10^6$ K. There is thermal equilibrium between the cold and warm phases. Measurements of Faraday rotation and dispersion measurements of pulsars give mean magnetic field strength of $2 \, \mu$G in the solar neighborhood (Ruzmaikin & Sokolov 1977; Inoue & Tabara 1981). According to recent data on synchrotron polarization, the Galactic magnetic field strength is up to $\sim 5 \, \mu$G (Planck Collaboration et al. 2016b). Zeeman-splitting measurements of the 21 cm absorption line show that median value of the magnetic field is of $6 \, \mu$G in diffuse clouds with density $\sim 10 - 100 \, \mathrm{cm}^{-3}$ (Heiles & Troland 2005;

Crutcher et al. 2010; Heiles & Haverkorn 2012). These values correspond to plasma beta $\lesssim 1$, therefore the magnetic field plays important role in the dynamics of the ISM.

The CNM is non-homogeneous (see review by Snow & McCall 2006). The densest parts of the CNM are the complexes of molecular clouds or giant molecular clouds (GMC). GMC demonstrate filamentary structure, i.e. they have the form of filaments and sheets (see review André et al. 2014). The CNM also contains translucent clouds with densities $n \sim 500 \, \mathrm{cm}^{-3}$ and temperatures $15 - 30$ K, and diffuse clouds with $n = 10 - 500 \, \mathrm{cm}^{-3}$ and temperatures $30 - 100$ K. Moreover, the tiny scale atomic structures (TSAS) are observed in the CNM with typical sizes $10 - 1000$ au, $n = 10^3 - 10^4 \, \mathrm{cm}^{-3}$, $T = 15 - 100$ K (Dieter et al. 1976; Heiles 1997; Stanimirović et al. 2010; Stanimirović & Zweibel 2018). Nature of the small-scale structures in the CNM is still under debate.

The formation of various structures in diffuse ISM is explained by the action of different instabilities and turbulence under the influence of the magnetic field (see reviews Dudorov 1991; Elmegreen & Scalo 2004; Hennebelle et al.

⋆ E-mail: dudorov@csu.ru (AED)
† E-mail: fominso@csu.ru (SOF)
‡ E-mail: khaibrakhmanov@csu.ru (SAKh)

2009; Dudorov & Khaibrakhmanov 2017). Separation of the ISM into cold clouds surrounded by warm gas is caused by thermal instability (Field 1965; Pikel'ner 1967 with English translation Pikel'ner 1968; Field et al. 1969). The turbulence in the ISM arises due to Kelvin-Helmholtz instability that may develop in the converging flows from supernova remnants. The structures in diffuse ISM can be a product of the interplay between compressible turbulence and heating and cooling processes in the neutral interstellar gas. Some fraction of thermally unstable gas can be produced by turbulent motions. The collision of turbulent flows can initiate condensation of warm neutral medium into cold neutral clouds with the fraction of cold gas, as well as the fraction of thermally unstable gas (see Banerjee et al. 2009; Hennebelle et al. 2009, and references therein).

Thermal instability develops usually as isobaric, isochoric and isentropic modes. The unstable isobaric and isochoric modes are dynamical ones. The unstable isentropic mode is either dynamical or overstable (Field 1965).

Various applications of thermal instability were considered in a number of papers. Defouw (1970) have shown that the partially ionized hydrogen that is cooled by free-bound emissions can be thermally unstable. Frozen-in magnetic field decreases the increments of the isobaric thermal instability in the direction nonparallel to the magnetic field lines (Heyvaerts 1974). Ohmic and ambipolar diffusion weaken the influence of magnetic field on the isobaric mode (Heyvaerts 1974; Massaglia et al. 1985; Nejad-Asghar & Ghanbari 2003; Stiele et al. 2006). The friction between ions and neutrals can weaken thermal instability in two-fluid plasma with magnetic field (Fukue & Kamaya 2007).

Several authors investigated the isentropic instabilities in the ISM. Oppenheimer (1977) discussed general conditions for the isentropic instability in molecular clouds. Nakariakov et al. (2000) investigated the isentropic instability in weak non-linear approximation. The isentropic instability can develop in the atomic zone of photodissociation regions (Krasnobaev & Tagirova 2017).

Yoneyama (1973) and Glassgold & Langer (1976) investigated thermal-chemical instability. In the case of ionization/recombination processes this instability was called as a thermo-reactive instability (Yoneyama 1973; Corbelli & Ferrara 1995).

Flannery & Press (1979) investigated ionization-coupled acoustic instability in the cold diffuse ISM. They have shown that thermally stable gas can be acoustically unstable, and discussed the applications of this instability to star formation. This instability has the following physical mechanism. Let an element of gas is compressed by a sound wave on the intermediate time-scale between the cooling and recombination time-scales in the thermally stable medium. If the cooling time-scale is shorter than the recombination time-scale then gas behaves almost isothermally with constant ionization fraction. For the time-scale of the sound wave larger than recombination time-scale ions begin to recombine at the end of compression. In some astrophysical cases cooling is produced by collisional excitation of gas particles with electrons and neutrals. The cooling decreases with decreasing ionization fraction, leading to additional pressure increase in the element of gas. During the rarefaction phase the pressure excess produces

work on the ambient gas and hence amplifies the wave. In this process some part of the energy of cosmic rays, X-rays and ultraviolet radiation transforms into the energy of growing acoustic waves.

In this paper, we follow Dudorov & Stepanov (1999) and generalize approach of Flannery & Press (1979) by including magnetic field into consideration. In this case, magnetosonic modes arise. We investigate the instability of magnetosonic waves taking into account heating/cooling and ionization/recombination processes and call further this instability as a magnetic ionization-thermal instability (MITI). We consider possible applications of MITI, such as the formation of TSAS and the generation of turbulence in the diffuse ISM.

The paper is organized in the following way. In Section 2, we derive the dispersion equation for the system of magnetohydrodynamical equations using the method of small perturbations. In Section 3, the analytical criteria for the instability are derived. The numerical solutions of the dispersion equation are presented in Section 4. Main results and their applications are discussed in Section 5.

2 DISPERSION EQUATION

Let us consider stability of homogeneous infinite magnetized medium with respect to small perturbations.

The behaviour of such a medium may be described by the following set of magnetohydrodynamical (MHD) equations:

$$\frac{\partial \rho}{\partial t} + \nabla \cdot (\rho \mathbf{v}) = 0, \tag{1}$$

$$\frac{\partial \mathbf{v}}{\partial t} + (\mathbf{v} \cdot \nabla) \mathbf{v} = -\frac{\nabla P}{\rho} + \frac{1}{4\pi\rho} (\nabla \times \mathbf{B}) \times \mathbf{B}, \tag{2}$$

$$\frac{\partial \mathbf{B}}{\partial t} = \nabla \times (\mathbf{v} \times \mathbf{B}), \tag{3}$$

$$\rho \left[\frac{\partial \varepsilon}{\partial t} + (\mathbf{v} \cdot \nabla) \varepsilon \right] + P \nabla \cdot \mathbf{v} = -\mathcal{L}(\rho, T, x), \tag{4}$$

$$\frac{\partial x}{\partial t} + (\mathbf{v} \cdot \nabla) x = -\mathcal{R}(\rho, T, x), \tag{5}$$

$$P = \frac{\rho k_B T}{\mu m_H}, \qquad \varepsilon = \frac{P}{(\gamma - 1)\rho}, \tag{6}$$

where $\mathcal{L} = \Lambda(\rho, T, x) - \Gamma(\rho, T, x)$ is the net cooling function per unit volume, $\Lambda(\rho, T, x)$ is the cooling function, $\Gamma(\rho, T, x)$ is the heating function, $x = n_e/n$ is the ionization fraction, n_e is the electrons concentration, n is the gas density, $\mathcal{R} = \mathcal{R}(\rho, T, x)$ is the net recombination rate per atom (equal to the difference between recombination and ionization rates), k_B is the Boltzmann constant, μ is the molecular weight of the gas, and adiabatic index $\gamma = 5/3$. All the remaining variables are used in their usual notation.

The system of equations (1–6) takes into account non-stationary ionization and thermal processes and allows us to investigate the effect of magnetic field on the ionization-thermal instability. We neglect direct viscous and diffusional

processes.The net cooling function depends not only on the temperature and density but also on the ionization fraction. Equation of non-stationary ionization (5) contains the source term $\mathcal{R}(\rho, T, x)$ depending on the ionization fraction, temperature and density.

We investigate MITI using the method of small perturbations. In the equilibrium state $\mathcal{L}(\rho, T, x) = 0$ and $\mathcal{R}(\rho, T, x) = 0$, although the derivatives of $\mathcal{L}$ and $\mathcal{R}$ are non-zero. The gas is ionized by cosmic rays and is heated by cosmic rays, X-rays and electronic photoemission from the dust grains. The cooling is produced by collisional excitation of fine structure levels of the carbon ions C II by electrons and neutral hydrogen (Wolfire et al. 1995).

We express each variable in the system of Equations (1–6) as a sum $f = f_0 + f'$, where f_0 describes the unperturbed state, and $|f'| \ll |f_0|$ is the small perturbation. Linearising the system of Equations (1–6), we obtain the following system of equations for the small perturbations

$$\frac{\partial \rho'}{\partial t} + \rho_0 \nabla \cdot \mathbf{v} = 0, \tag{7}$$

$$\frac{\partial \mathbf{v}'}{\partial t} = -c_T^2 \left(\frac{\nabla \rho'}{\rho_0} + \frac{\nabla T'}{T_0} \right) + \frac{1}{4\pi\rho_0} \left(\nabla \times \mathbf{B}' \right) \times \mathbf{B}_0, \tag{8}$$

$$\frac{\partial \mathbf{B}'}{\partial t} = \nabla \times \left(\mathbf{v}' \times \mathbf{B}_0 \right), \tag{9}$$

$$\frac{1}{T_0} \frac{\partial T'}{\partial t} + (\gamma - 1)\nabla \cdot \mathbf{v}' = -\frac{\gamma - 1}{\rho_0 c_T^2} \left(\mathcal{L}_\rho \rho' + \mathcal{L}_T T' + \mathcal{L}_x x' \right), \tag{10}$$

$$\frac{\partial x'}{\partial t} = -\left(\mathcal{R}_\rho \rho' + \mathcal{R}_T T' + \mathcal{R}_x x' \right), \tag{11}$$

where $\mathcal{L}_\rho$ and $\mathcal{R}_\rho$, $\mathcal{L}_T$ and $\mathcal{R}_T$, $\mathcal{L}_x$ and $\mathcal{R}_x$ mean partial derivatives of the net cooling and net recombination functions with respect to density, temperature and ionization fraction, respectively, $c_T = \sqrt{k_B T_0 / \mu m_H}$ is the isothermal sound speed.

Consider the perturbations in the form

$$f' = f_1 \exp(i\mathbf{k} \cdot \mathbf{r} + \sigma t), \tag{12}$$

where f_1 is the perturbation amplitude, $\mathbf{k}$ is the wave vector and

$$\sigma = \sigma_R + i\omega, \tag{13}$$

σ_R is the increment (or decrement) and ω is the frequency. Substituting the perturbations (12) into the system of Equations (7–11), we obtain the linear algebraic system

$$\sigma \frac{\rho_1}{\rho_0} + i \left(\mathbf{k} \cdot \mathbf{v}_1 \right) = 0, \tag{14}$$

$$\sigma \mathbf{v}_1 = -i\mathbf{k} c_T^2 \left(\frac{\rho_1}{\rho_0} + \frac{T_1}{T_0} \right) + \frac{i}{4\pi\rho_0} \left(\mathbf{k} \times \mathbf{B_1} \right) \times \mathbf{B}_0, \tag{15}$$

$$\sigma \mathbf{B}_1 = i\mathbf{k} \times \left(\mathbf{v}_1 \times \mathbf{B}_0 \right), \tag{16}$$

$$\sigma \frac{T_1}{T_0} + i(\gamma - 1)(\mathbf{k} \cdot \mathbf{v}_1) = -c_T \left(k_\rho \frac{\rho_1}{\rho_0} + k_T \frac{T_1}{T_0} + k_x \frac{x_1}{x_0} \right). \tag{17}$$

$$\sigma \frac{x_1}{x_0} = -c_T \left(q_\rho \frac{\rho_1}{\rho_0} + q_T \frac{T_1}{T_0} + q_x \frac{x_1}{x_0} \right). \tag{18}$$

We define the characteristic thermal wave numbers in Equation (17) following Field (1965)

$$k_\rho = \frac{(\gamma - 1)}{c_T^3} \left(\frac{\partial \mathcal{L}}{\partial \rho} \right)_{T,x}, \quad k_T = \frac{(\gamma - 1)T_0}{\rho_0 c_T^3} \left(\frac{\partial \mathcal{L}}{\partial T} \right)_{\rho,x},$$

$$k_x = \frac{(\gamma - 1)x_0}{\rho_0 c_T^3} \left(\frac{\partial \mathcal{L}}{\partial x} \right)_{\rho,T},$$

and the characteristic ionization wave numbers in Equation (18)

$$q_\rho = \frac{\rho_0}{x_0 c_T} \left(\frac{\partial \mathcal{R}}{\partial \rho} \right)_{T,x}, \quad q_T = \frac{T_0}{x_0 c_T} \left(\frac{\partial \mathcal{R}}{\partial T} \right)_{\rho,x}, \quad q_x = \frac{1}{c_T} \left(\frac{\partial \mathcal{R}}{\partial x} \right)_{\rho,T}.$$

We also define following modified characteristic thermal wave numbers:

$$(k_T)_\rho = k_T - \frac{q_T}{q_x} k_x, \quad (k_\rho)_T = k_\rho - \frac{q_\rho}{q_x} k_x,$$

$$(k_T)_P = (k_T)_\rho - (k_\rho)_T.$$

Resolving equations (14, 17, 18) with respect to ρ_1/ρ_0, T_1/T_0 and x_1/x_0, we reduce Equation (15) to

$$\sigma \mathbf{v}_1 + \frac{(\mathbf{k} \cdot \mathbf{v}_1)}{\sigma} \widetilde{\gamma} c_T^2 \mathbf{k} = \frac{i}{4\pi\rho_0} \left(\mathbf{k} \cdot \mathbf{B}_1 \right) \mathbf{B}_0, \tag{19}$$

where

$$\widetilde{\gamma} = \frac{\gamma \sigma^2 + c_T \left(k_T - k_\rho + \gamma q_x \right) \sigma + c_T^2 q_x (k_T)_P}{\sigma^2 + c_T \left(k_T + q_x \right) \sigma + c_T^2 q_x (k_T)_\rho} \tag{20}$$

plays the role of 'effective' adiabatic index. Expanding the double vector products in Equation (16) and substituting $\mathbf{B}_1$ from Equation (16) into Equation (19), we obtain the following characteristic vector equation for the velocity perturbation:

$$\sigma^2 \mathbf{v}_1 + (\mathbf{k} \cdot \mathbf{v}_1) \left[\widetilde{\gamma} c_T^2 \mathbf{k} + \mathbf{v}_A \times (\mathbf{k} \times \mathbf{v}_A) \right] - \left(\mathbf{k} \cdot \mathbf{v}_A \right) \left[\mathbf{v}_A \times (\mathbf{k} \times \mathbf{v}_1) \right] = 0, \tag{21}$$

where $\mathbf{v}_A = \mathbf{B}_0 / \sqrt{4\pi\rho_0}$ is the Alfvèn speed.

Equation (21) describes the waves with various relative orientations of vectors $\mathbf{k}, \mathbf{v}_1$, and $\mathbf{v}_A$. The effects of thermal and magnetic pressures in this equation are described by the second term, while the third one describes the magnetic tension effects.

Equation (21) reduces to the dispersion equation for the Alfvèn waves in the case $\mathbf{v}_1 \perp \mathbf{k}$,

$$\sigma^2 + (\mathbf{k} \cdot \mathbf{v}_A)^2 = 0.$$

This equation does not include the effects of ionization-recombination and heating-cooling processes, as the Alfvèn waves are incompressible ones in linear approximation. We do not consider them in the following.

Making separately vector and scalar products of $\mathbf{k}$ with Equation (21), we obtain a homogeneous system of linear

algebraic equations with unknowns $(\mathbf{k} \times \mathbf{v}_1)$ and $(\mathbf{k} \cdot \mathbf{v}_1)$. Resolving this system, we obtain a dispersion equation for the magnetosonic and dynamical modes:

$$\sigma^4 + \sigma^2 \left(\widetilde{\gamma} c_T^2 + v_A^2 \right) k^2 + \widetilde{\gamma} c_T^2 v_A^2 k^4 \cos^2 \theta = 0, \tag{22}$$

where θ is the angle between the wave vector and the unperturbed magnetic field.

Substituting Expression (20) into Equation (22), we obtain a dispersion equation of the 6-th order

$$\sigma^6 + c_T \left(k_T + q_x \right) \sigma^5 + c_T^2 \left[(\gamma + A) k^2 + q_x \left(k_T \right)_\rho \right] \sigma^4 +$$
$$c_T^3 k^2 \left[(1 + A) k_T - k_\rho + (\gamma + A) q_x \right] \sigma^3 +$$
$$c_T^4 k^2 \left[A \gamma k^2 \cos^2 \theta + q_x \left(k_T \right)_\rho (1 + A) - q_x \left(k_\rho \right)_T \right] \sigma^2 + \tag{23}$$
$$A c_T^5 k^4 \cos^2 \theta \left(k_T - k_\rho + \gamma q_x \right) \sigma +$$
$$A c_T^6 q_x \left(k_T \right)_P k^4 \cos^2 \theta = 0,$$

where

$$A = v_A^2 / c_T^2 = 2/\beta \tag{24}$$

is the Alfvèn number, $\beta = 8\pi P/B^2$ is the plasma beta.

3 INSTABILITY CRITERIA

3.1 Asymptotic analysis

The dispersion equation (23) is the polynomial of the sixth order and it cannot be solved analytically in general. We can find out all of its solutions in the limiting cases of small and large wave numbers by means of asymptotic analysis following Heyvaerts (1974).

3.1.1 Small wavelength limit

Let us consider the case of small wavelengths. The solutions of Equation (23) include two slow magnetosonic modes

$$\sigma_{s\pm} = -\frac{c_T \left(v_f^2 - \gamma c_T^2 \right)}{2\gamma \left(v_f^2 - v_s^2 \right)} \left[k_T (\gamma - 1) + k_\rho \right] \pm i k v_s, \tag{25}$$

two fast magnetosonic modes

$$\sigma_{f\pm} = -\frac{c_T \left(\gamma c_T^2 - v_s^2 \right)}{2\gamma \left(v_f^2 - v_s^2 \right)} \left[k_T (\gamma - 1) + k_\rho \right] \pm i k v_f, \tag{26}$$

and the pair of dynamical modes

$$\sigma_{P\pm} = \frac{c_T}{2\gamma} \left[- \left(k_T - k_\rho + \gamma q_x \right) \right] \pm$$
$$\frac{c_T}{2\gamma} \sqrt{\left(k_T - k_\rho + \gamma q_x \right)^2 - 4\gamma q_x \left(k_T \right)_P}, \tag{27}$$

where

$$v_{f,s} = \sqrt{\frac{1}{2} \left[\gamma c_T^2 + v_A^2 \pm \sqrt{\left(\gamma c_T^2 + v_A^2 \right)^2 - 4\gamma c_T^2 v_A^2 \cos^2 \theta} \right]} \tag{28}$$

are the fast (v_f) and slow (v_s) magnetosonic speeds. The fast and slow waves correspond to '+' and '−' signs under the square root in Equation (28), respectively.

Heyvaerts (1974) found the solutions similar to (25–26) taking into account Joule and thermal conductivity terms. The magnetosonic modes (25–26) are unstable if

$$k_T (\gamma - 1) + k_\rho < 0. \tag{29}$$

Inequality (29) is the criterion for the isentropic instability (Field 1965). It is not satisfied in the conditions of diffuse H I clouds that we consider in this paper (Oppenheimer 1977).

Equations (25–26) show that the ionization and recombination processes do not affect the magnetosonic modes at small wavelengths.

Modes (27) are unstable if one of inequalities

$$k_T - k_\rho + \gamma q_x < 0, \tag{30}$$

$$\left(k_T \right)_P < 0, \tag{31}$$

or both of them are satisfied. Inequality (30) corresponds to the Field's (1965) criterion for the isobaric thermal instability, but it takes into account the stabilization due to recombinations. Inequality (31) corresponds to the thermal-reactive instability criterion (Yoneyama 1973; Corbelli & Ferrara 1995). When inequality (30) is satisfied and (31) is not, then Equation (23) has two unstable roots instead of one root of the dispersion equation of Field (1965). This effect occurs due to an additional degree of freedom that appears from the ionization equation.

The pair of modes (27) can transform to oscillatory ones. It depends on the sign of the expression under the square root in Equation (27). If

$$\left(k_T - k_\rho + \gamma q_x \right)^2 - 4\gamma q_x \left(k_T \right)_P < 0$$

then Equation (27) becomes

$$\sigma_{P\pm} = -\frac{c_T}{2\gamma} \left(k_T - k_\rho + \gamma q_x \right) \pm$$
$$i \frac{c_T}{2\gamma} \sqrt{\left| \left(k_T - k_\rho + \gamma q_x \right)^2 - 4\gamma q_x \left(k_T \right)_P \right|}. \tag{32}$$

Modes (32) develop as the standing waves, as their frequency does not depend on the wave number and their group wave speed equals zero.

3.1.2 Large wavelength limit

In the long wavelength limit, the solutions of Equation (23) are two slow magnetosonic modes

$$\sigma_{s\pm} = -\frac{c_T}{2} \frac{Q_s}{q_x \left(k_T \right)_\rho \left(k_T \right)_P} \xi k^2 \pm i k v_s, \tag{33}$$

two fast magnetosonic modes

$$\sigma_{f\pm} = -\frac{c_T}{2} \frac{Q_f}{q_x \left(k_T \right)_\rho \left(k_T \right)_P} \xi k^2 \pm i k v_f, \tag{34}$$

and two dynamical modes

$$\sigma_{\rho\pm} = \frac{c_T}{2} \left[-(k_T + q_x) \pm \sqrt{(k_T + q_x)^2 - 4 q_x \left(k_T \right)_\rho} \right], \tag{35}$$

where

$$\xi = q_x \left[(\gamma - 1)(k_T)_\rho + (k_\rho)_T \right] + k_T (k_\rho)_T - k_\rho (k_T)_\rho, \tag{36}$$

$$Q_s = \frac{v_s^2 \left(v_f^2 - \gamma_0 c_T^2\right)}{c_T^2 \left(v_f^2 - v_s^2\right)}, Q_f = \frac{v_f^2 \left(\gamma_0 c_T^2 - v_s^2\right)}{c_T^2 \left(v_f^2 - v_s^2\right)}, \tag{37}$$

and

$$\gamma_0 = \frac{(k_T)_P}{(k_T)_\rho} \tag{38}$$

is the effective adiabatic index in the small frequency limit. The wave speeds of the fast and slow waves are expressed by Equation (28) with γ_0 substituted instead of γ.

The fast and slow magnetosonic modes (33–34) are unstable if

$$\frac{\xi}{q_x(k_T)_\rho(k_T)_P} < 0. \tag{39}$$

In the isobarically and isochorically stable medium condition (39) becomes

$$\xi < 0. \tag{40}$$

This is a criterion of MITI. Expressions (36) and (39) show that this criterion does not include magnetic field, and it is the same as for the ionization-coupled acoustic instability of Flannery & Press (1979).

The growth rates of the slow and fast magnetosonic modes (33), (34) are determined by the dimensionless factors Q_s and Q_f that depend on the Alfvèn number (24) through v_s and v_f. If $Q_s/Q_f > 1$ then the slow mode has faster growth rate than the fast one. In Fig. 1 , we plot the dependencies of Q_s and Q_f on A for various values of angle θ. Fig. 1 shows that the fast mode dominates the slow one at any θ in the case of weak magnetic field $A \ll 1$ (or $\beta \gg 1$ according to Equation (24)). The slow mode dominates the fast one at $\theta < \pi/4$ in the case strong magnetic field $A \gg 1$ ($\beta \ll 1$).

Modes (35) are unstable if

$$k_T + q_x < 0 \tag{41}$$

or

$$(k_T)_\rho < 0. \tag{42}$$

Criterion (41) corresponds to the isochoric thermal instability of Field (1965) with stabilization due recombinations. Inequality (42) describes the thermal-reactive instability in the large wavelength limit (Corbelli & Ferrara 1995).

3.2 Critical wave numbers and frequencies

The asymptotic analysis carried out in Section 3.1 shows that the magnetosonic modes in the isobarically, isochorically and isentropically stable medium are unstable only if condition (40) for ξ from (36) is satisfied. In this case, the magnetosonic mode is unstable only at the wave numbers less than some critical one. In order to determine the critical wave numbers and corresponding frequencies for the slow and fast magnetosonic modes, we represent σ in the form (13). The critical wave numbers and frequencies correspond to the case $\sigma_R = 0$. We substitute $\sigma = i\omega$ into the dispersion equation (23) and obtain the following critical wave number and corresponding critical frequency:

$$k_{cr}^2 = -\frac{q_x c_T^2 \xi}{u_{f,s}^2 \left[k_T (\gamma - 1) + k_\rho\right]}, \tag{43}$$
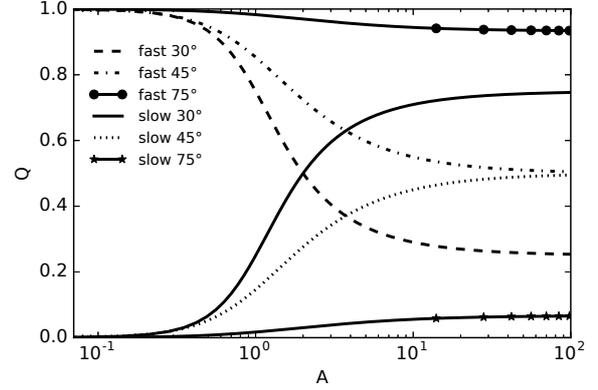
Figure 1. The dependencies of the dimensionless factors Q_f (dashed line, dot-dashed line and solid line with rounds) and Q_s (solid line, dotted line and solid line with stars) on the Alfvèn number A. The curves are plotted for $\theta = 30°, 45°, 75°$ (see legend) and adiabatic index $\gamma_0 = 1$.

$$\omega_{cr}^2 = -\frac{q_x c_T^2 \xi}{k_T (\gamma - 1) + k_\rho}, \tag{44}$$

where $u_{f,s}$ are the fast and slow magnetosonic speeds determined according to Equation (28) with γ_{cr} substituted instead of γ. And

$$\gamma_{cr} = \frac{k_T - k_\rho + \gamma q_x}{k_T + q_x}$$

is the effective adiabatic index for the waves with the critical frequency ω_{cr}. It should be noted that frequency ω_{cr} in Equation (44) is the same for the fast and slow magnetosonic waves.

Formulae (43-44) determine the regions of the parameter space in which the magnetosonic waves can be amplified, $k < k_{cr}$ or $\omega < \omega_{cr}$.

4 NUMERICAL SOLUTION OF THE DISPERSION EQUATION

In this section, we solve numerically the dispersion equation (23) and analyse its solutions. We apply the Bairstow's method to find out the roots. This method uses Newton-Raphson iterations to extract the complex roots of a polynomial by pairs.

The results of the solution of the dispersion equation (23) are shown in Figs. 2–8 for the mean Galactic values of magnetic field $B = 2 \cdot 10^{-6}$ G, ionization rate of cosmic rays $\xi_{CR} = 10^{-17}$ s^{-1} and heating rate $h = 5 \cdot 10^{-26}$ erg s^{-1} (Spitzer & Tomasko 1968).

The heating function can be expressed as $\Gamma(\rho) = nh$. The cooling function is calculated according to Wolfire et al. (1995)

$$\Lambda(\rho, T, x) = 2.54 \cdot 10^{-14} X_C f_{C\,II} \left[\gamma^{H_0} (1 - x) + \gamma^e x\right] n^2 \times$$
$$\exp\left(-\frac{92}{T}\right) \text{ erg s}^{-1} \text{ cm}^{-3}, \tag{45}$$

where the carbon abundance $X_C = 3 \cdot 10^{-4}$ and fraction

$f_{C\ II}$ = 1. Values of the collisional de-excitation rate coefficients for collisions with neutral hydrogen γ^{H_0} = 8.86 · 10^{-10} cm^3 s^{-1} and electrons γ^e = $\gamma^e(T)$ are taken from Wolfire et al. (1995). Equation (45) includes cooling only due the collisional excitations of fine structure levels C II with hydrogen atoms and electrons.

For the net recombination rate $\mathcal{R}(\rho, T, x)$ we take

$$\mathcal{R}(\rho, T, x) = x^2 n\alpha(T) - \xi_{CR}(1-x), \quad (46)$$

where $\alpha(T) = 4.1 \cdot 10^{-12} \left(T/10^2\right)^{-0.6}$ cm^3 s^{-1} is the rate of radiative recombinations taken from Flannery & Press (1979).

The density and ionization fraction are calculated for given temperature using equations (45–46) in the equilibrium state $\mathcal{L}(\rho, T, x) = 0$ and $\mathcal{R}(\rho, T, x) = 0$. For temperatures $T = 30 - 100$ K we obtain $n \sim 150 - 15$ cm^{-3} and $x \sim 10^{-5} - 10^{-4}$ that correspond to diffuse clouds. Corresponding plasma beta lies in range from 4 to 1.4.

For example, the characteristic wave numbers are k_ρ = 159.1 pc^{-1}, k_T = 199.0 pc^{-1}, k_x = 20.2 pc^{-1}, q_ρ = 1.6 pc^{-1}, q_T = −1.0 pc^{-1} and q_x = 3.2 pc^{-1} at $T = 70$ K. For these wave numbers criterion (40) is satisfied.

In Fig. 2–5, we show the solutions for various temperatures (70 and 95 K) and angles $\theta = \pi/6$, $\pi/3$. The a-panels of each figure show the growth rates of the unstable modes ($\sigma_R > 0$); the b-panels show the absolute values of the decrements of the decaying modes ($\sigma_R < 0$) and the c-panels show the frequencies (ω).

In Fig. 2, we depict the solutions of Equation (23) for $T = 70$ K and $\theta = \pi/6$. In this case, curves 1 and 2 describe slow magnetosonic waves (SMSW) propogating in the opposite directions. Curves 3 and 4 correspond to fast magentosonic waves (FMSW) propogating in the opposite directions. And curves 5, 6 are the pair of the stable isobarical modes. Growth rates of SMSW and FMSW proportional to k^2 for small wave numbers according to Equations (33, 34). The growth rate of SMSW is positive for the wave numbers $k < 10$ pc^{-1}. Fig. 2 shows that the growth rate of SMSW increases with k from 10^{-11} yr^{-1} at $k \approx 0.04$ pc^{-1} to maximum $5 \cdot 10^{-8}$ yr^{-1} at $k \approx 5$ pc^{-1} and then rapidly goes to zero at $k = k_{cr}^{SMSW} \approx 10$ pc^{-1}. At $0 < k < 0.03$ pc^{-1} SMSW and FMSW are unstable but their growth rates are less than 10^{-11} yr^{-1}. SMSW are stable at $k > k_{cr}^{SMSW}$. The decrement of SMSW increases from 0 to 10^{-5} yr^{-1} in the range $k = [k_{cr}^{SMSW}, 100]$ pc^{-1} and remains nearly constant at larger k. The growth rate and decrement of FMSW depend on k in similar way as for SMSW. FMSW are unstable at $k < k_{cr}^{FMSW} \approx 4$ pc^{-1} and has maximum growth rate $\approx 3 \cdot 10^{-9}$ yr^{-1}.

As it was shown with the help of asymptotic analysis (see Section 3.1), the ionization and recombination processes do not affect the instability of the magnetosonic waves for the short wavelength perturbations (Section 3.1.1). This instability correspond to the isentropic thermal instability (29) and it does not develop under the conditions considered in our paper.

The period of a magnetosonic wave equals $t_0 = \lambda/(c_s^2 + v_A^2)^{1/2}$, where λ is the wavelength and c_s is the sound speed. The characteristic ionization time-scale equals $t_{ion} = 1/\xi_{CR} \sim 10^9$ yrs for $\xi_{CR} = 10^{-17}$ s^{-1}. The period of the magnetosonic wave with small wavelength is much less than the ionization time. The ionization fraction does not change
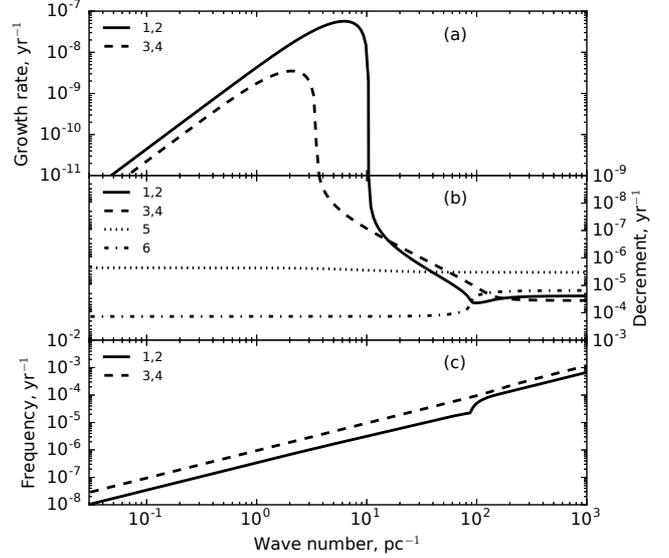

Figure 2. Two slow magnetosonic waves (solid lines 1,2), two fast magnetosonic waves (dashed lines 3,4) and pair of stable modes with $\omega = 0$ (dotted and dot-dashed lines 5,6) are solutions of the dispersion equation (23) for $T = 70$ K and $\theta = \pi/6$. Panel (a): the growth rates of unstable modes ($\sigma_R > 0$). Panel (b): the decrements of stable modes ($\sigma_R < 0$). Panel (c): the frequencies (ω) on the wave number.

significantly over the period of the wave, and the wave amplification mechanism does not work. Hence, the magnetosonic waves decay at small λ.

At small k magnetosonic waves are unstable but growth rates could be too low for instability to develop. In this case the characteristic time-scale of a magnetosonic wave is much more than the cooling and recombination time-scales. The gas evolves to the ionization-thermal equilibrium, and cools too fast avoiding the rarefaction phase.

SMSW modes have ten times faster maximum growth rate than FMSW, and SMSW are unstable in wider range of wavelengths under considered conditions. The decrements of SMSW and FMSW are almost equal to each other at large wave numbers. The frequencies of SMSW and FMSW increase with k according to a power law from $10^{-8} - 10^{-7}$ yr^{-1} at $k = 0.1$ pc^{-1} to 10^{-3} yr^{-1} at $k = 1000$ pc^{-1}.

Fig. 3 shows that general behaviour of the solutions for $\theta = \pi/3$ is similar to the one depicted in Fig. 2. Maximum growth rate of SMSW shifts towards larger k, while maximum growth rate of FMSW moves towards smaller k, as compared to the case with $\theta = \pi/6$. The FMSW modes slightly dominate the SMSW ones at small wave numbers, $k \lesssim k_{cr}^{FMSW} \approx 3$ pc^{-1}. At higher wave numbers, FMSW decays, while the SMSW mode is unstable up to $k \lesssim k_{cr}^{SMSW} \approx 20$ pc^{-1}. The slight dominance of SMSW over FMSW for small wave numbers at $\theta = \pi/6$ and conversely at $\theta = \pi/3$ confirms the results of asymptotic analysis (see Section 3.1.2). The maximum growth rates are of the same order as in the case $\theta = \pi/6$.

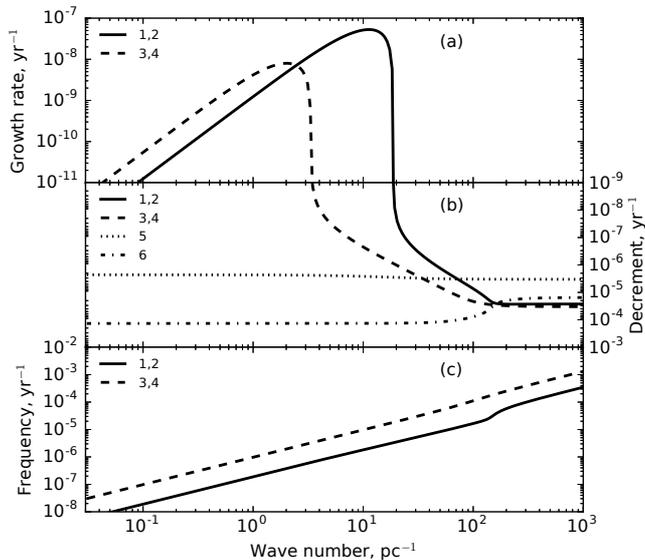We pay attention to SMSW as a mode with the largest growth rate and define the right bound for instability as

Figure 3. Same as in Fig. 2, but for $T = 70$ K and $\theta = \pi/3$.

Table 1. Critical wave numbers $k_{\rm cr}$ (in units of pc^{-1}) of the slow magnetosonic waves for various values of T and θ.

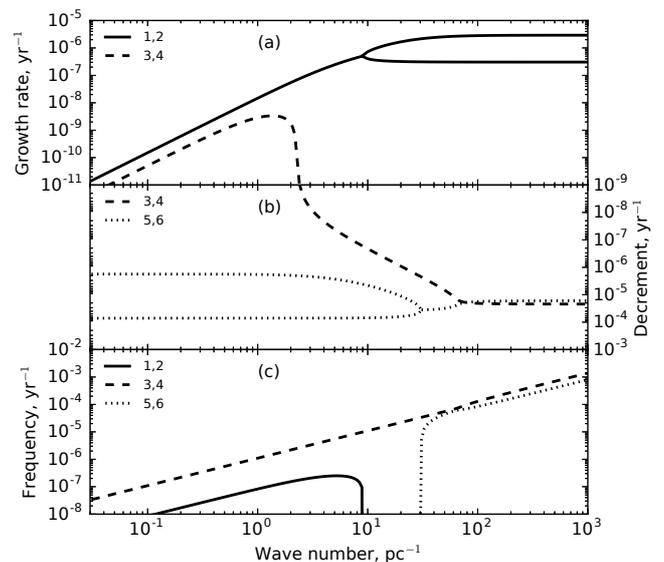|	10°	20°	30°	40°	50°	60°	70°	80°
30 K	14.7	16.3	18.6	22.0	27.1	35.8	53.4	106.3
40 K	12.9	14.1	16.1	19.0	23.4	30.8	45.9	91.4
50 K	11.2	12.0	13.4	15.7	19.2	25.2	37.3	74.3
60 K	10.2	10.9	12.1	13.9	16.9	22.1	32.7	64.9
70 K	10.3	10.8	11.9	13.6	16.5	21.4	31.5	62.5
80 K	12.4	13.0	14.2	16.1	19.4	25.0	36.7	72.6

Figure 4. Same as in Fig. 2, but for $T = 95$ K and $\theta = \pi/6$. Here two unstable SMSW (solid lines 1,2) transform into the pair of unstable ionization-thermal modes, and pair of stable modes with $\omega = 0$ (dotted lines 5,6) transform into the pair of stable SMSW towards larger wave numbers.

$k_{cr} = k_{\rm cr}^{\rm SMSW}$. In Table 1, we listed values of $k_{\rm cr}$ for the slow magnetosonic waves as a function of temperature (different rows) and angle θ (different columns) calculated using analytic formulae (43). The values of $k_{\rm cr}$ correspond to the right boundary of the instability domain for the magnetosonic waves. Table 1 shows that $k_{\rm cr}$ increases with θ. The dependence of $k_{\rm cr}$ on T is non-monotonic and has minimum at $T \approx 65$ K for $\theta = 10° - 80°$. The values of the critical wave numbers $k_{\rm cr}^{\rm SMSW}$ found in the numerical solution of the dispersion equation (see Fig. 2, 3) agree with the values in Table 1. The values of $k_{\rm cr}$ lie between ≈ 10 and ≈ 100 pc^{-1}, that corresponds to the waves with $\lambda \approx [0.01, 0.1]$ pc.

Figs. 4–5 show the solutions of the dispersion equation for the case $T = 95$ K. The transition to the isobaric thermal instability occurs near this temperature.

At this temperature, the solutions 1 and 2 correspond to the unstable slow magnetosonic modes at $k < 8.8$ pc^{-1} ($\theta = \pi/6$) and $k < 15.6$ pc^{-1} ($\theta = \pi/3$). At larger wave numbers, these solutions describe the unstable ionization-thermal modes. Solutions 5 and 6 (dotted lines) correspond to two decaying modes at $k < 30.6$ pc^{-1} ($\theta = \pi/6$) and $k < 41.8$ pc^{-1} ($\theta = \pi/3$) that transform into the pair of decaying slow magnetosonic modes at larger wave numbers. There is a 'gap' of wave numbers at which the slow magnetosonic waves do not propagate ($8.8 < k < 30.6$ pc^{-1} at $\theta = \pi/6$ and $15.6 < k < 41.8$ pc^{-1} at $\theta = \pi/3$). Beyond the 'gap' at large wave numbers, the slow magnetosonic wave speed appreciably increases. FMSW (curves 3, 4) remains unaffected by the transition into the thermally unstable region of parameter space and behave the similar way as in the cases depicted in Figs. 2–3.

For the small wave numbers SMSW have faster growth rate than FMSW for $\theta = \pi/6$ (Figs. 2, 4) and vice versa for $\theta = \pi/3$ (Figs. 3, 5) which proves the asymptotic analysis for the $A \approx 1$ or $\beta \approx 2$ (see Fig. 1).

The dependencies of the growth rates of the unstable slow magnetosonic and isobaric modes on the wave number are shown in Fig. 6(a) for various values of temperature in the range 35 - 120 K. Corresponding frequencies are plotted in Fig. 6(b). The dependences are calculated for $\theta = \pi/6$. Fig. 6(a) shows that the maximum growth rates of the unstable oscillatory and dynamical modes increase with temperature. At $T = 35$ K the minimal growth time of the slow magnetosonic mode is $\sim 5 \cdot 10^8$ yr at the wavelength $\lambda \sim 0.1$ pc. At $T = 70$ K the corresponding values are $\sim 2 \cdot 10^7$ yr and ~ 0.15 pc, respectively.

In the range of temperatures 35-70 K, the slow magnetosonic instability develops if the wave number is less than some threshold value $k_{\rm cr}$ in accordance with Equation (43). Critical wave number $k_{\rm cr} \approx 5 - 10$ pc^{-1} in the cases depicted in Fig. 6. The growth rate increases with increasing temperature. At $T = 92$ K, the instability has a character of standing waves with growth time $\approx 1.1 \cdot 10^6$ yr at the small wavelengths. At $T = 95$ K (solid line with rounds in Fig. 6), two slow magnetosonic waves transform to the dynamical modes with different growth rates for $k \gtrsim 10$ pc^{-1}.

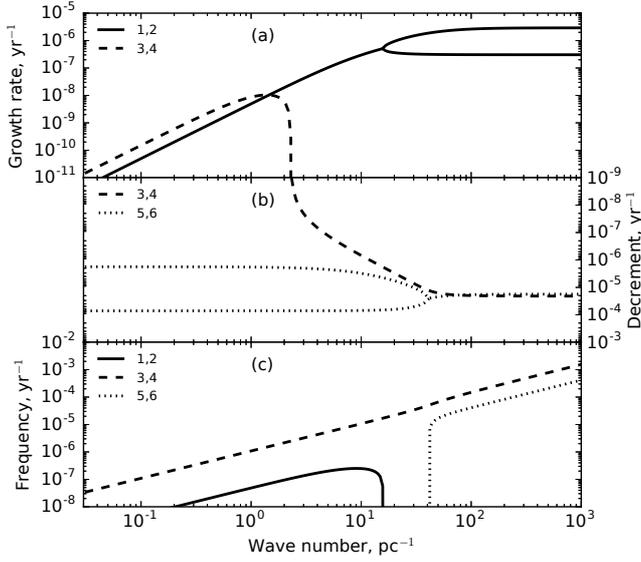Our calculations show that the branching point, where

Figure 5. Same as in Fig. 4, but for $T = 95$ K and $\theta = \pi/3$.

two dynamical modes transform into the pair of the oscillatory ones, shifts towards the smaller wave numbers, as the temperature increases and reaches zero at $T \approx 100$ K. At $T = 120$ K, the unstable slow magnetosonic modes disappear completely, and there remains only one unstable isobaric mode (solid line with triangles in Fig. 6).

In Fig. 7, we plot the dependence of the growth rates of FMSW on k for various T in the unstable region. The curves are plotted for $\theta = \pi/6$. The growth rates of FMSW are smaller in comparison with the ones of SMSW. FMSW achieve their maximum growth rates at $\lambda \approx 0.2 - 1$ pc with corresponding growth time approximately $5 \cdot 10^8$ yr. The unstable FMSW do not transform into isobaric instability in comparison with the SMSW modes.

In Fig. 8, we plot the maximum growth rates of the unstable slow magnetosonic modes (panel a) and corresponding wave numbers (panel b) versus temperature for various values of the angle θ. Fig. 8 shows that the maximum growth rate of the SMSW modes very weakly depends on θ and grows with growing temperature. The instability of SMSW exists only at $T > 25$ K. At $T > 92$ K, $k_{max} \to \infty$ that corresponds to the transformation of the unstable SMSW into the dynamical ionization-thermal modes. The wave number k_{max} increases with θ, as Fig. 8(b) shows.

In Table 2, we show maximum growth rate, σ_{max} (column 6), minimum growth time, σ_{max}^{-1} (column 7), and corresponding characteristic wavelengths λ_{max} of acoustic waves ($B = 0$) and SMSW (column 8) for various magnetic field strengths (column 1) and cosmic ray ionization rates (column 2). Corresponding equilibrium values of density and ionization fraction are listed in columns 3 and 4, respectively. Values presented in Table 2 are calculated for $\theta = \pi/4$. Table 2 shows that magnetic field decreases the growth rates of SMSW as compared to the unstable acoustic waves. The growth time of SMSW decreases with increasing magnetic field strength and cosmic ray ionization rate. The growth time is of $4 \cdot 10^6$ yr for $\xi_{CR} = 5 \cdot 10^{-17}$ and $T = 70$ K.
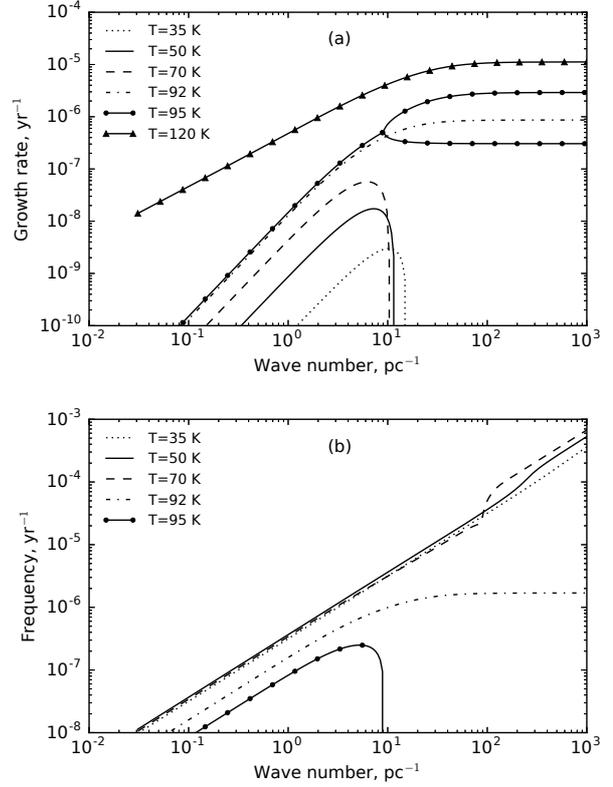

Figure 6. The dependencies of the growth rates σ_R (panel (a)) and the frequencies ω (panel (b)) of the unstable slow magnetosonic modes and dynamical modes on the wave number for various values of temperature in the range (35-120 K). The angle between magnetic field **B** and wave vector **k** $\theta = \pi/6$.
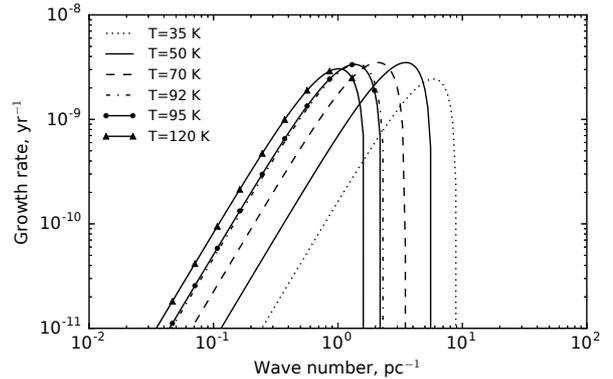

Figure 7. The dependencies of the growth rates σ of the unstable fast magnetosonic modes on the wave number for different values of temperature in the range (35-120 K) for the angle between magnetic field **B** and wave vector **k** $\theta = \pi/6$.

Dependence of σ_{max} on magnetic field strength can be analysed using asymptotic formulae from Section 3.1.2. The growth rates of SMSW and FMSW are the real parts of $\sigma_{s\pm}$ and $\sigma_{f\pm}$ in Equations (33-34). In Figure 9, we plot dependences of these growth rates on the Alfvèn number for various angles θ, $T = 70$ K, $h = 5 \cdot 10^{-26}$ erg s^{-1}, $\xi_{CR} = 5 \cdot 10^{-17}$ s^{-1}, $k = 10$ pc^{-1}. The growth rate of the

Table 2. Dependence of maximum increments, minimum growth times and corresponding wavelengths of acoustic waves and SMSW on the characteristics of the medium.

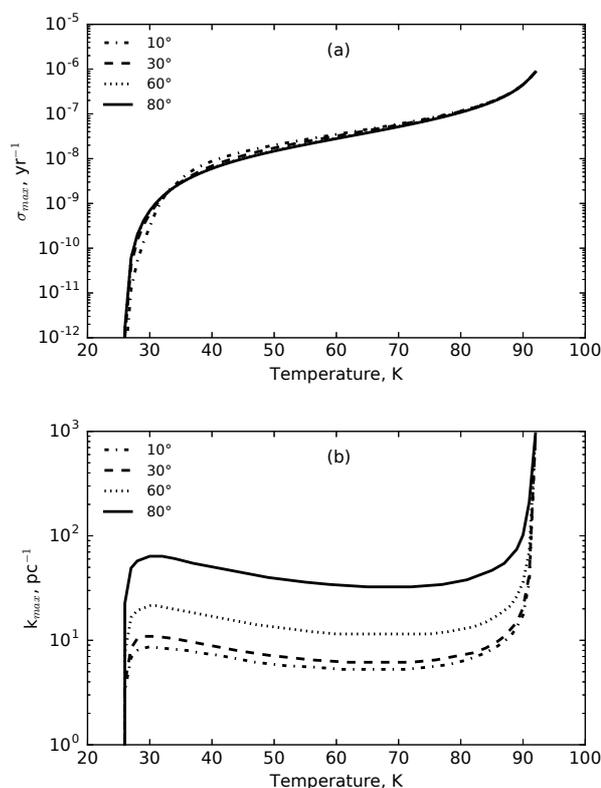| B, μG (1)	ξ_{CR}, s^{-1} (2)	T, K (3)	n, cm^{-3} (4)	x (5)	σ_{max}, yr^{-1} (6)	σ_{max}^{-1}, Myr (7)	λ_{max}, pc (8)
0	$1 \cdot 10^{-17}$	50	42	$2 \cdot 10^{-4}$	$2.1 \cdot 10^{-8}$	48	0.94
		70	24	$3 \cdot 10^{-4}$	$6.0 \cdot 10^{-8}$	17	1.05
	$5 \cdot 10^{-17}$	50	36	$5 \cdot 10^{-4}$	$8.9 \cdot 10^{-8}$	11	0.45
		70	20	$7 \cdot 10^{-4}$	$2.4 \cdot 10^{-7}$	4.1	0.50
2	$1 \cdot 10^{-17}$	50	42	$2 \cdot 10^{-4}$	$1.6 \cdot 10^{-8}$	63	0.57
		70	24	$3 \cdot 10^{-4}$	$5.6 \cdot 10^{-8}$	18	0.69
	$5 \cdot 10^{-17}$	50	36	$5 \cdot 10^{-4}$	$7.1 \cdot 10^{-8}$	14	0.25
		70	20	$7 \cdot 10^{-4}$	$2.2 \cdot 10^{-7}$	4.5	0.31
6	$1 \cdot 10^{-17}$	50	42	$2 \cdot 10^{-4}$	$2.0 \cdot 10^{-8}$	50	0.63
		70	24	$3 \cdot 10^{-4}$	$5.9 \cdot 10^{-8}$	17	0.75
	$5 \cdot 10^{-17}$	50	36	$5 \cdot 10^{-4}$	$8.3 \cdot 10^{-8}$	12	0.31
		70	20	$7 \cdot 10^{-4}$	$2.4 \cdot 10^{-7}$	4.2	0.38

Figure 8. The dependencies of the maximum growth rate (a) and the corresponding wave number (b) of the unstable slow magnetosonic modes on temperature for different values of the angle θ.

Figure 9. The dependences of the increments of FMSW and SMSW on the Alfvèn number for various angles θ, T = 70 K, h = 5 · 10^{-26} erg s^{-1}, ξ_{CR} = 5 · 10^{-17} s^{-1}, k = 10 pc^{-1}. Horizontal solid line depicts the increment of the unstable acoustic wave.

unstable acoustic wave is also shown, which corresponds to the case $B = 0$. The growth rate of the acoustic wave does not depend on A and equals 5×10^{-7} yr^{-1}. Figure 9 shows that the growth rates of SMSW and FMSW are less than the growth rate of the acoustic wave, which reflects stabilizing effect of the magnetic field. The growth rates of SMSW and FMSW have similar behaviour as factors Q_s and Q_f depicted in Figure 1. The growth rate of SMSW rapidly increases with A for the case of a weak magnetic field ($A \ll 1$) and asymptotically
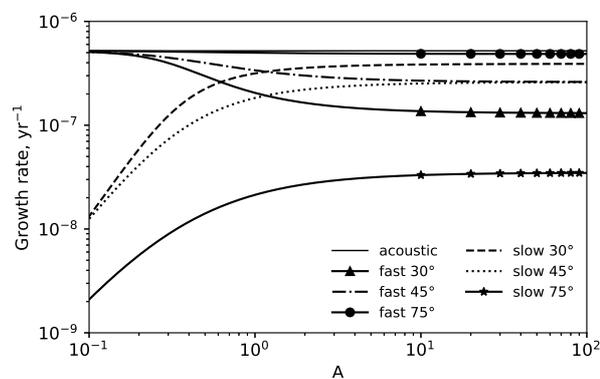
tends to constant value for a strong magnetic field ($A \gg 1$). The growth rate of FMSW decreases with A at $A \ll 1$ and is nearly constant at $A \gg 1$. Increase of the growth rate of SMSW with magnetic field strength is explained by the fact that the perturbation of magnetic pressure has opposite sign as compared to the perturbation of gas pressure in SMSW (see, for example, Somov 2012). Therefore, the magnetic pressure of SMSW does not prevent pressure and density increase at the compression phase. On the contrary, magnetic pressure and gas pressure add up in FMSW, and the magnetic field prevents plasma compression. The growth rate of SMSW decreases with increasing angle θ. SMSW do not propagate in the direction perpendicular to the magnetic field. For small angles θ and $A > 1$, the growth rate of SMSW tends to the growth rate of the acoustic wave. The growth rate of FMSW increases with the angle θ.

5 CONCLUSION

We investigated the stability of the CNM with frozen-in magnetic field with the help of small perturbations. It was considered that the gas is heated by cosmic rays, X-rays and

electronic photoemission from the dust grains, while cooling is provided by collisional excitation of fine structure levels C II with hydrogen atoms and electrons. Ionization state of the CNM was determined from the balance between cosmic ray ionization and radiative recombinations.

Derived dispersion relation describes all modes of thermal instability (Field 1965), and in particular thermal-reactive modes (Yoneyama 1973; Corbelli & Ferrara 1995), ionization-coupled acoustic modes (Flannery & Press 1979). We focused on the instability of magnetosonic waves, that arise in presence of magnetic field, in thermally stable region, with temperature $35 < T < 95$ K and density $n \lesssim 10^3 \, \text{cm}^{-3}$. The instability is affected by heating/cooling and ionization/recombination processes, so we called it as a magnetic ionization-thermal instability (MITI).

The dispersion equation is investigated analytically in the cases of small and large wave numbers, as well as numerically in general case. Typical Galactic magnetic field strength, ionization rates by cosmic rays and the rates of heating by cosmic rays, X-rays and electronic photoemission from the dust grains are adopted in the calculations.

The asymptotic analysis and numerical solution of the dispersion equation show that MITI has the threshold behaviour in the CNM. The magnetosonic modes can be unstable only at the wave number less than a critical one, $k < k_{\text{cr}}$. We obtain the expressions for the critical wave numbers, k_{cr}, of the slow and fast magnetosonic modes. The critical wave number for the slow magnetosonic waves increases with the angle θ between the magnetic field and wave vector. Typical values of critical wave number k_{cr} lie in range $2 - 20$ pc^{-1} depending on θ and gas temperature.

In the limit of large wavelengths, the unstable slow magnetosonic waves have larger growth rate than the fast magnetosonic waves for the angle between magnetic field lines and wave vector $\theta < \pi/4$ and Alfvèn number $A \gg 1$. In the isobarically unstable region ($T \geq 100$ K) the slow magnetosonic modes are stable, but the unstable fast magnetosonic modes have small growth rates $\sigma_{\text{R}} \lesssim 10^{-9}$ yr^{-1} and do not play significant role in the dynamics of medium.

Depending on the angle θ in the range from 0 to $\pi/2$, the slow magnetosonic modes have the most unstable wavelengths $\lambda_{\text{max}} \approx 0.1 - 0.15$ pc. The growth time of the unstable slow magnetosonic modes decreases with magnetic field strength and cosmic ray ionization rate. It lies in range from ~ 4 to ~ 60 Myr. For example, the growth time is of ~ 4 Myr for $B = 6 \, \mu$G, $\xi_{\text{CR}} = 5 \cdot 10^{-17}$ s^{-1} and $T = 70$ K. This time is less than the characteristic time of Galaxy spiral pattern rotation period of about ≈ 200 Myr in the solar neighbourhood (according to data from Reid et al. 2014). Therefore, MITI can develop over the dynamical time of Galaxy evolution. The formation of clouds in the CNM is often explained by the action of the interstellar turbulence and shock waves (see review Elmegreen & Scalo 2004). The turbulent velocity at the scale l_0 can be estimated as $v_{\text{turb}} = 1 (l_0/1 \, \text{pc})^\delta$ km s^{-1}, where $\delta \sim 0.4 - 0.6$ (see e.g. Larson 1981; Dudorov 1991; Mac Low & Klessen 2004; Ballesteros-Paredes et al. 2007; Kritsuk et al. 2013). Therefore, the characteristic time-scale of the interstellar turbulence $\tau_0 = l_0/v_{\text{turb}}$ is of order of few Myr in diffuse clouds with sizes $l_0 < 10$ pc and $\tau_0 \gtrsim 10^7$ yr for clouds with $l_0 \gtrsim 10$ pc. These times are comparable to the growth time of MITI. We propose that MITI can lead to the formation of conden-

sations, such as TSAS, in the diffuse CNM, along with the turbulence. The condensations would have sizes more than $0.05 - 0.5$ pc under typical conditions in the CNM.

The growth of the slow magnetosonic waves with the wave vector almost perpendicular to the magnetic field lines, $\theta = \pi/2$, can lead to the formation of condensations elongated in the direction of magnetic field. This instability can be one of the possible mechanisms of the formation of filament-like clouds with typical width of 0.1 pc threaded by parallel magnetic field in the ISM (see André et al. 2014; Planck Collaboration et al. 2016a).

We also propose that MITI at the non-linear stage can lead to the generation of MHD wave turbulence. The dependence of velocity dispersion on spatial scale has the from of power law $\Delta v \propto l^{1/2}$ in this case (Sagdeev & Galeev 1969). That type of turbulence can one of the possible mechanisms of the condensations of TSAS. This suggestion must to be checked with 3-D numerical modeling of non-linear stage of MITI. We plan to study the development of MITI at higher densities and stronger magnetic field in future, to investigate the role of MITI in interstellar molecular clouds and accretion disks of young stars. We also suggest that mechanism of MITI can be applied to H II regions.

ACKNOWLEDGEMENTS

REFERENCES

André P., Di Francesco J., Ward-Thompson D., Inutsuka S.-I., Pudritz R. E., Pineda J. E., 2014, Protostars and Planets VI, pp 27–51

Ballesteros-Paredes J., Klessen R. S., Mac Low M.-M., Vázquez-Semadeni E., 2007, Protostars and Planets V, pp 63–80

Banerjee R., Vázquez-Semadeni E., Hennebelle P., Klessen R. S., 2009, MNRAS, 398, 1082

Corbelli E., Ferrara A., 1995, ApJ, 447, 708

Crutcher R. M., Wandelt B., Heiles C., Falgarone E., Troland T. H., 2010, ApJ, 725, 466

Defouw R. J., 1970, ApJ, 161, 55

Dieter N. H., Welch W. J., Romney J. D., 1976, ApJ, 206, L113

Dudorov A. E., 1991, Soviet Ast., 35, 342

Dudorov A. E., Khaibrakhmanov S. A., 2017, Open Astronomy, 26, 285

Dudorov A. E., Stepanov C. E., 1999, Astronomical and Astrophysical Transactions, 18, 101

Elmegreen B. G., Scalo J., 2004, ARA&A, 42, 211

Field G. B., 1965, ApJ, 142, 531

Field G. B., Goldsmith D. W., Habing H. J., 1969, ApJ, 155, L149

Flannery B. P., Press W. H., 1979, ApJ, 231, 688

Fukue T., Kamaya H., 2007, ApJ, 669, 363

Glassgold A. E., Langer W. D., 1976, ApJ, 204, 403

Heiles C., 1997, ApJ, 481, 193

Heiles C., Haverkorn M., 2012, SSRv, 166, 293

Heiles C., Troland T. H., 2005, ApJ, 624, 773

Hennebelle P., Low M.-M. M., Vazquez-Semadeni E., 2009, Diffuse interstellar medium and the formation of molecular clouds. Cambridge University Press, pp 205–227, doi:10.1017/CBO9780511575198.010

Heyvaerts J., 1974, A&A, 37, 65

Inoue M., Tabara H., 1981, PASJ, 33, 603

Krasnobaev K. V., Tagirova R. R., 2017, MNRAS, 469, 1403

Kritsuk A. G., Lee C. T., Norman M. L., 2013, MNRAS, 436, 3247

Larson R. B., 1981, MNRAS, 194, 809

Mac Low M.-M., Klessen R. S., 2004, RvMP, 76, 125

Massaglia S., Ferrari A., Bodo G., Kalkofen W., Rosner R., 1985, ApJ, 299, 769

McKee C. F., Ostriker J. P., 1977, ApJ, 218, 148

Nakariakov V. M., Medoza-Briceño C. A., Ibáñez S. M. H., 2000, ApJ, 240, 488

Nejad-Asghar M., Ghanbari J., 2003, MNRAS, 345, 1323

Oppenheimer M., 1977, ApJ, 211, 400

Pikel'ner S. B., 1967, ARep, 44, 915

Pikel'ner S. B., 1968, Soviet Ast., 11, 737

Planck Collaboration et al., 2016a, A&A, 586, A135

Planck Collaboration et al., 2016b, A&A, 596, A103

Reid M. J., et al., 2014, ApJ, 783, 130

Ruzmaikin A. A., Sokolov D. D., 1977, Ap&SS, 52, 365

Sagdeev R. Z., Galeev A. A., 1969, Nonlinear Plasma Theory

Snow T. P., McCall B. J., 2006, ARA&A, 44, 367

Somov B. V., ed. 2012, Plasma Astrophysics, Part I Astrophysics and Space Science Library Vol. 391, doi:10.1007/978-1-4614-4283-7.

Spitzer Jr. L., Tomasko M. G., 1968, ApJ, 152, 971

Stanimirović S., Zweibel E. G., 2018, ARA&A, 56, 489

Stanimirović S., Weisberg J. M., Pei Z., Tuttle K., Green J. T., 2010, ApJ, 720, 415

Stiele H., Lesch H., Heitsch F., 2006, MNRAS, 372, 862

Wolfire M. G., Hollenbach D., McKee C. F., Tielens A. G. G. M., Bakes E. L. O., 1995, ApJ, 443, 152

Yoneyama T., 1973, PASJ, 25, 349